

SAMwave: Wavelet-Driven Feature Enrichment for Effective Adaptation of Segment Anything Model

Saurabh Yadav^{*1}
saurabhy@iiitd.ac.in

Avi Gupta^{*1}
avig@iiitd.ac.in

Koteswar Rao Jerripothula^{2,1}
kotesrj@iitk.ac.in

¹ IIIT Delhi
New Delhi, India

² IIT Kanpur
Kanpur, India

Abstract

The emergence of large foundation models has propelled significant advances in various domains. The Segment Anything Model (SAM), a leading model for image segmentation, exemplifies these advances, outperforming traditional methods. However, such foundation models often suffer from performance degradation when applied to complex tasks for which they are not trained. Existing methods typically employ adapter-based fine-tuning strategies to adapt SAM for tasks and leverage high-frequency features extracted from the Fourier domain. However, Our analysis reveals that these approaches offer limited benefits due to constraints in their feature extraction techniques. To overcome this, we propose **SAMwave**, a novel and interpretable approach that utilizes the wavelet transform to extract richer, multi-scale high-frequency features from input data. Extending this, we introduce complex-valued adapters capable of capturing complex-valued spatial-frequency information via complex wavelet transforms. By adaptively integrating these wavelet coefficients, SAMwave enables SAM’s encoder to capture information more relevant for dense prediction. Empirical evaluations on four challenging low-level vision tasks demonstrate that SAMwave significantly outperforms existing adaptation methods. This superior performance is consistent across both the SAM and SAM2 backbones and holds for both real and complex-valued adapter variants, highlighting the efficiency, flexibility, and interpretability of our proposed method for adapting segment anything models.

1 Introduction

Large vision models [15, 17, 19] have become the dominant solution for numerous computer vision tasks, significantly advancing fields like semantic segmentation [28, 33] and object detection. However, their substantial parameter counts, while enabling high performance on their trained tasks, lead to sub-optimal generalization to other related problems, a challenge

particularly evident in low-level vision tasks. For instance, while SAM [28] excels at semantic segmentation, it struggles with tasks like camouflaged object detection. The difficulty of developing a single, universally high-performing model for all low-level vision tasks has led to growing interest in adapting large models [8, 33, 34, 40, 51, 69]. Another common fine-tuning strategy is finetuning; however, it faces several challenges, including catastrophic forgetting [10, 9, 6, 21, 58, 51] and the reliance on large-scale datasets for adequate adaptation.

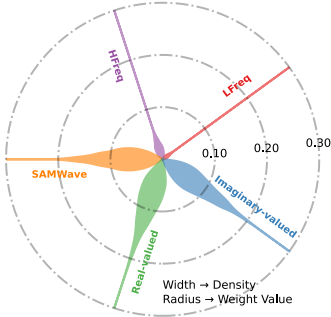


Figure 1: Learned weights for previous high frequency extraction method, compared with SAMWave’s real and complex adapter weights. Unlike previous method, SAMWave’s weights are not concentrated around 0.

In this work, we investigate the optimal adaptation of large models to related tasks, focusing particularly on **SAM**, which comprises of a powerful encoder and a prompt-conditioned decoder. We hypothesize that the encoder can produce a sufficiently rich latent representation, such that the decoder can generate effective segmentation mask for new task—given appropriate supervision. Previous works [8, 37] have shown the efficacy of providing high-frequency features to the encoder for adapting a frozen decoder. These methods are typically performed by transforming input images into the Fourier domain and applying a predefined mask to emphasise high-frequency components. Different images possess varying frequency distributions, and a fixed mask leads to suboptimal feature selection. Our empirical study, presented in Tab. 1, supports this observation—demonstrating that simply inverting the mask yields comparable performance across tasks. Fig. 1 further illustrates this issue. This motivates our departure from rigid, predefined Fourier-domain masks toward a more adaptive feature selection mechanism. To this end, we propose a novel high-frequency feature extraction method using wavelet transform, which offers superior spatial and frequency localization [29, 50, 62]. Specifically, we extract horizontal (I_{lh}), vertical (I_{hl}), and diagonal (I_{hh}) features from an image I , combining them into a high-frequency image $I_{HF} = I_{lh} + I_{hl} + I_{hh}$, which provides finer details and texture to the encoder. Wavelet transform is advantageous due to its ability to capture both frequency and spatial information, allowing for a more precise representation of image details compared to Fourier-based methods. We further extend this approach with complex wavelet transforms and complex-valued adapters. Complex-valued representations offer a more comprehensive way to capture image information, potentially leading to improved feature extraction and adaptation, as demonstrated in various applications[56, 74]. We are the first to show the adaptation of vision foundational models using a complex-valued approach. Our contributions are summarized as follows: **1** We demonstrate the limitations of using the Fourier domain with predefined masks for high-frequency feature extraction. **2** We introduce a Wavelet High-Frequency (WHF) module that leverages the wavelet transform for effective fine-tuning. **3** We propose a complex-valued extension of our method using complex wavelet transform and complex-valued adapters. **4** Our experiments show significant performance improvements over existing tuning methods for SAM and SAM2 across four low-level tasks.

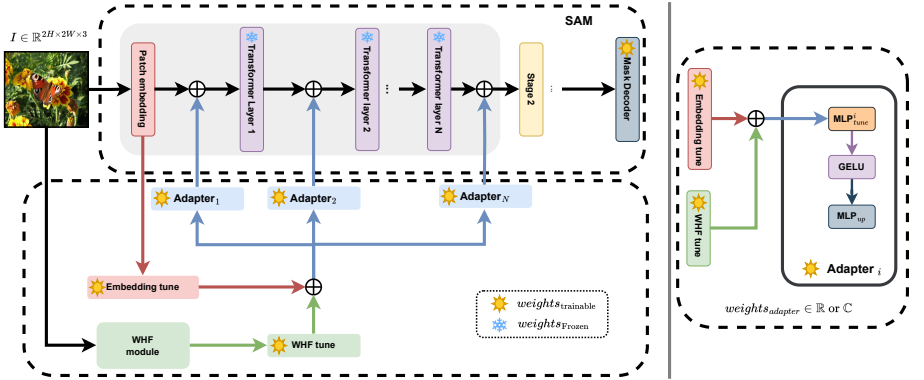


Figure 2: Overview of SAMwave for low-level vision tasks. **Right** shows that the image is passed through SAM and our WHF (wavelet high frequency) module, where the high-frequency features are extracted. The extracted details are then combined with patch embeddings obtained from the transformer encoder. Note that the encoder is frozen; we only updated the decoder for our training. **Left** shows the overview of a single adapter used; for complex adapters, we replace the weights of MLP layers with complex values.

2 Related Work

Visual Adapters. The paradigm of adapting large pre-trained models for downstream tasks, initially popular in NLP [27], has effectively extended to computer vision [9, 35]. Recent work has shown its applicability to vision foundation models like SAM [28], notably through visual prompting methods [7, 37]. While prior adaptation methods often prioritize global context, our work focuses on incorporating crucial local, high-frequency information via wavelets to enhance SAM’s performance on low-level vision tasks.

Low-level Vision Tasks. Our work addresses several low-level vision tasks where fine-grained details are critical for accurate localization. **Camouflaged Object Detection (COD)** involves distinguishing objects seamlessly blended into their background [17, 19, 32], requiring models to capture subtle boundary cues [38, 76]. **Defocus Blur Detection (DBD)** aims to identify out-of-focus image regions, relying on variations in blur kernels that are often captured by local features like edges [27, 37, 35]. **Shadow Detection (SD)** requires distinguishing shadows from true objects, often involving analyzing illumination patterns and local spatial context [23, 83]. **PolyP Detection (PD)** involves delineating polyp regions from endoscopic images, thereby assisting clinicians in the early detection and treatment of colorectal abnormalities [35, 63]. **Forgery Detection (FD)** focuses on locating manipulated pixels, where inconsistencies in noise levels or texture often manifest as high-frequency anomalies [17, 38]. While some methods [37] use generic high-frequency components for low-level tasks, we propose a more principled approach using specific wavelet decompositions to provide targeted local feature guidance to SAM for these diverse low-level vision challenges.

3 Method

In this section, we describe our proposed network SAMwave. The idea is to leverage the high-frequency features obtained from wavelet transform and use them to guide the Segment-Anything model (SAM) [28] for more precise segmentation in various tasks.

Table 1: Result of low frequency (LFreq) & high frequency (HFreq) on camouflaged object detection on three separate datasets. We also show the difference in the performance of both approaches.

	CHAMELEON				CAMO				COD10K			
	$S_m \uparrow$	$\mathcal{E}_\phi \uparrow$	$\mathcal{F}_\beta^w \uparrow$	$\mathcal{M} \downarrow$	$S_m \uparrow$	$\mathcal{E}_\phi \uparrow$	$\mathcal{F}_\beta^w \uparrow$	$\mathcal{M} \downarrow$	$S_m \uparrow$	$\mathcal{E}_\phi \uparrow$	$\mathcal{F}_\beta^w \uparrow$	$\mathcal{M} \downarrow$
HFreq	0.896	0.919	0.824	0.033	0.847	0.873	0.765	0.070	0.883	0.918	0.801	0.025
LFreq	0.888	0.903	0.830	0.034	0.824	0.843	0.765	0.078	0.872	0.901	0.803	0.027
	+0.008	+0.016	-0.006	+0.001	+0.023	+0.030	0.000	+0.008	+0.009	+0.017	-0.002	+0.002

3.1 Motivation for High-Frequency Feature Utilization

Precise segmentation, particularly the accurate delineation of object boundaries, is a challenging task that fundamentally relies on capturing fine-grained image details. These details are predominantly encoded within the high-frequency components of the image signal. Therefore, effectively leveraging high-frequency features is crucial for achieving high-quality segmentation masks.

Previous methods aiming to incorporate high-frequency information, such as those in [4, 37], have often relied on extracting these features in the Fourier domain using a predefined, fixed mask. However, a significant limitation of this "one mask fits all" approach is its inability to adapt to the diverse characteristics and varying distributions of high-frequency information present across different images and tasks. Consequently, a static Fourier mask may not effectively isolate the relevant high-frequency cues necessary for robust fine-grained segmentation in all scenarios.

To investigate the efficacy of this fixed-mask approach for capturing essential high-frequency information, we conducted an empirical study. We compared the performance using features extracted via the standard high-frequency mask (HFreq) against those extracted by inverting this mask to obtain low-frequency features (LFreq). Our experiments focused on the challenging task of camouflaged object detection, and the results are summarized in Tab. 1. While HFreq shows superior performance on 9 out of 12 metrics compared to LFreq, a closer examination reveals that the average performance gain offered by HFreq is remarkably small, merely **0.009**. This marginal difference, despite high frequencies theoretically being more aligned with boundary information, suggests that a fixed Fourier mask is not an optimal strategy for extracting discriminative high-frequency features that significantly enhance segmentation performance across varied data. This observation motivates the need for a more adaptive and effective approach to harness high-frequency information for guiding models like SAM towards more precise segmentation.

3.2 SAM as the Backbone

Our SAMwave framework employs the Segment-Anything Model (SAM) [28] as its core backbone, leveraging its robust pre-trained capabilities for various segmentation tasks. SAM comprises three main components: an image encoder, a prompt encoder, and a mask decoder.

The image encoder, a pre-trained ViT-H/16, processes the input image $I \in \mathbb{R}^{H \times W \times 3}$ to produce dense embeddings $E_{\text{img}} \in \mathbb{R}^{\frac{H}{16} \times \frac{W}{16} \times 256}$. These embeddings are spatially downsampled by $16\times$ and have 256 channels after a 1×1 convolution. The prompt encoder processes input prompts (such as dense features from our method) typically using convolutions, and these prompt embeddings are element-wise added to E_{img} . The mask decoder, a lightweight transformer-based network inspired by [8, 10], takes the combined embeddings and predicts the final segmentation mask via upsampling and a linear classifier.

In SAMWave, we freeze the weights of the pre-trained image encoder and train only the parameters of the mask decoder to adapt SAM’s segmentation generation to the task-specific guidance.

3.3 Wavelet High-Frequency Module (WHF)

The Wavelet High-Frequency (WHF) module extracts rich high-frequency spatial features using the Discrete Wavelet Transform (DWT). Given an input image $I \in \mathbb{R}^{H \times W \times 3}$, we first resize it to $I' \in \mathbb{R}^{2H \times 2W \times 3}$. This upsampling compensates for the DWT’s inherent downsampling, ensuring output subbands match the original $H \times W$ resolution.

Applying a 2D DWT to I' decomposes it into four subbands at $H \times W \times 3$ resolution: I'_{ll} (approximation), I'_{lh} (horizontal details), I'_{hl} (vertical details), and I'_{hh} (diagonal details). $I' \xrightarrow{\text{DWT}} \{I'_{ll}, I'_{lh}, I'_{hl}, I'_{hh}\}$. Focusing on fine details, we exclude the low-frequency I'_{ll} subband and combine the high-frequency detail subbands ($I'_{lh}, I'_{hl}, I'_{hh}$) to form the composite high-frequency map I_{HF} . $I_{HF} = I'_{lh} + I'_{hl} + I'_{hh} \in \mathbb{R}^{H \times W \times 3}$ captures edge and texture information (Fig. 3). This map is then projected to a D_{embed} channel dimension.

A key advantage of this wavelet-based approach is its inherent flexibility. While we describe the process using standard real-valued DWT, the WHF module can seamlessly incorporate complex wavelet transforms, such as the Dual-Tree Complex Wavelet Transform (DT-CWT)[69]. The core procedural steps—resizing, wavelet decomposition into subbands, selection and combination of high-frequency subbands, and linear projection—remain identical. The only change lies in the specific wavelet basis functions used in the decomposition, allowing for adaptation to properties captured by complex wavelets[64] (e.g., phase information, shift invariance) without altering the module’s overall structure.

3.4 SAMwave Architecture

SAMwave enhances SAM’s segmentation capabilities by integrating learned high-frequency wavelet features *via* lightweight adapters. As illustrated in Fig. 2, the architecture consists of three key modules—Embedding Tune, WHF Tune, and Adapters—which are integrated into the SAM backbone.

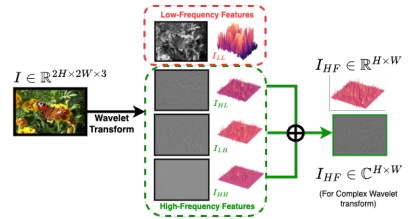


Figure 3: An overview of the WHF module, we first use the wavelet transform to obtain high- and low-frequency features. Then, we combine the high-frequency features to create a feature map, which is then used to provide finer details in the image.

Embedding Tune: This module generates a learned spatial feature map $\psi_{PE} \in \mathbb{R}^{\frac{H}{16} \times \frac{W}{16} \times \gamma}$ from SAM’s image encoder embeddings \mathbf{F}_{emb} using a learnable MLP layer $\phi_{PE}(\cdot; \theta_{PE})$:

$$\psi_{PE} = \phi_{PE}(\mathbf{F}_{\text{emb}}; \theta_{PE})$$

WHF Tune: Complementary to ψ_{PE} , this module processes the high-frequency feature map I_{HF} from the WHF module (§3.3). I_{HF} can be real or complex depending on the wavelet. Since the features I_{HF} are 2D spatial features, they are divided into patches and projected using a convolution layer to obtain ψ_{whf} , matching ψ_{PE} ’s dimensions.

Real/Complex Adapters: Adapters are placed within SAM’s image encoder layers. For layer i , the adapter input is the channel concatenation $\Psi = [\psi_{PE}, \psi_{whf}] \in \mathbb{R}^{\frac{H}{16} \times \frac{W}{16} \times 2\gamma}$ (or complex). The output $\mathbf{P}^{(i)} \in \mathbb{R}^{\frac{H}{16} \times \frac{W}{16} \times C_{\text{img}}^i}$ is computed via:

$$\mathbf{P}^{(i)} = \phi_{up}^{(i)}(\sigma(\phi_{tune}^{(i)}(\Psi)))$$

$\psi_{tune}^{(i)}$ and $\psi_{up}^{(i)}$ are MLPs (standard or complex), and the activation function (σ) is GeLU (or split GeLU for complex). $\mathbf{P}^{(i)}$ is then added with the layer’s feature map $\mathbf{F}_{\text{img}}^i$:

$$\bar{\mathbf{F}}_{\text{img}}^{(i)} = \mathbf{F}_{\text{img}}^{(i)} + \mathbf{P}^{(i)}$$

In case of complex adapters, the real and imaginary parts of $\mathbf{P}^{(i)}$ are both added separately to $\mathbf{F}_{\text{img}}^{(i)}$. The $\mathbf{P}^{(i)}$ feature is obtained for each layer separately and then added to the respective layer’s feature map. This provides robustness to learn features required for adaptation.

SAMwave benefits from: 1) **Feature Complementarity:** combining SAM’s semantic features with explicit learned high-frequency details; 2) **Wavelet Flexibility:** easily integrates various wavelets, including complex ones with \mathbb{C} -Adapters to leverage properties like shift invariance and phase information for improved robustness on challenging tasks.

4 Experimental Details and Analysis

We evaluate our approach on four low-level vision tasks: camouflaged object detection, shadow detection, defocus blur detection, and polyp detection and compare the performance with current state-of-the-art methods. We also perform ablation studies to analyze the effectiveness of our approach.

4.1 Datasets and Evaluation Metrics

Camouflaged Object Detection. Following [1, 37], we evaluate on COD10K [1], CAMO [30], and CHAMELEON [60]. Metrics: S-measure (\mathcal{S}_m) [16], mean E-measure (\mathcal{E}_ϕ), weighted F-measure (\mathcal{F}_β^w) [43], and Mean Absolute Error (\mathcal{M}).





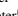

Shadow Detection. Following [1, 37], we evaluate on SBU [70] and ISTD [71]. Metric: Balanced Error Rate (BER).

Defocus Blur Detection. Following [1, 37], we evaluate on CUHK [59] and DUT [72]. Metrics: F-measure (\mathcal{F}_β) and Mean Absolute Error (\mathcal{M}).

PolyP Detection. Following [63], we evaluate on Kvasir-SEG [26], CVC-ClinicDB [8], ColonDB [63], ETIS [69]. Metrics: $MDice$ and $mIoU$.

Additional details about the datasets, along with training objectives and additional results on forgery detection, are provided in the *supplementary*.

Table 2: Comparison of Camouflaged Object Detection performance on three datasets against task-specific and finetuning methods. Our SAMwave approach demonstrates improved performance across all datasets compared to existing methods.(■: best, ■: second best)

Method	CHAMELEON				CAMO				COD10K			
	$S_m \uparrow$	$\varepsilon_\phi \downarrow$	$F_\beta \uparrow$	$M \downarrow$	$S_m \uparrow$	$\varepsilon_\phi \downarrow$	$F_\beta \uparrow$	$M \downarrow$	$S_m \uparrow$	$\varepsilon_\phi \downarrow$	$F_\beta \uparrow$	$M \downarrow$
SINet ⁽²⁰²⁰⁾ 	0.869	0.891	0.740	0.044	0.751	0.771	0.606	0.100	0.771	0.806	0.551	0.051
RankNet ⁽²⁰²¹⁾ 	0.846	0.913	0.767	0.045	0.712	0.791	0.583	0.104	0.767	0.861	0.611	0.045
JCOD ⁽²⁰²¹⁾	0.870	0.924	-	0.039	0.792	0.830	-	0.082	0.800	0.872	-	0.041
PFNet ⁽²⁰²¹⁾	0.882	0.942	0.810	0.033	0.782	0.852	0.695	0.085	0.800	0.868	0.660	0.04
FBNet ⁽²⁰²³⁾	0.888	0.939	0.828	0.032	0.783	0.839	0.702	0.081	0.809	0.889	0.684	0.035
FSPNet ⁽²⁰²³⁾	-	-	-	-	0.856	0.899	0.799	0.050	0.851	0.895	0.735	0.026
SAM ⁽²⁰²³⁾	0.727	0.734	0.639	0.081	0.684	0.687	0.606	0.132	0.783	0.798	0.701	0.050
SAM2 ⁽²⁰²⁴⁾ 	0.359	0.375	0.115	0.357	0.350	0.411	0.079	0.311	0.429	0.505	0.115	0.218
EVPt ⁽²⁰²³⁾ 	0.871	0.917	0.795	0.036	0.846	0.895	0.777	0.059	0.843	0.907	0.742	0.029
SAM-Adapter ⁽²⁰²³⁾ 	0.896	0.919	0.824	0.033	0.847	0.873	0.765	0.070	0.883	0.918	0.801	0.025
SAM2-Adapter ⁽²⁰²⁴⁾ 	0.915	0.955	0.889	0.018	0.855	0.909	0.810	0.051	0.899	0.950	0.850	0.018
SAM as Backbone												
Real-Valued Adapters												
Ours (daubechies (db))	0.922	0.947	0.856	0.023	0.865	0.903	0.790	0.057	0.900	0.936	0.824	0.021
Ours (coiflet (cf))	0.923	0.952	0.890	0.022	0.856	0.888	0.807	0.060	0.903	0.939	0.857	0.019
Ours (haar (ha))	0.923	0.954	0.866	0.023	0.868	0.905	0.798	0.056	0.899	0.934	0.819	0.022
Ours (symlet (sym))	0.915	0.947	0.845	0.027	0.846	0.880	0.777	0.067	0.897	0.938	0.822	0.021
Complex-Valued Adapters												
Ours (Symmetric-b (sy-b))	0.931	0.961	0.883	0.020	0.856	0.896	0.797	0.058	0.902	0.940	0.843	0.019
Ours (Symmetric-a (sy-a))	0.928	0.957	0.881	0.019	0.858	0.893	0.800	0.057	0.902	0.939	0.841	0.019
SAM2 as Backbone												
Real-Valued Adapters												
Ours (daubechies (db))	0.912	0.952	0.880	0.018	0.870	0.927	0.828	0.045	0.905	0.956	0.861	0.016
Ours (coiflet (cf))	0.917	0.963	0.883	0.017	0.866	0.923	0.824	0.048	0.905	0.957	0.862	0.016
Ours (haar (ha))	0.918	0.962	0.889	0.017	0.869	0.926	0.829	0.047	0.900	0.952	0.865	0.017
Ours (symlet (sym))	0.917	0.961	0.887	0.017	0.871	0.929	0.831	0.045	0.905	0.954	0.859	0.016
Complex-Valued Adapters												
Ours (Symmetric-b (sy-b))	0.917	0.966	0.890	0.016	0.864	0.921	0.824	0.049	0.902	0.955	0.858	0.017
Ours (Symmetric-a (sy-a))	0.917	0.960	0.881	0.019	0.864	0.921	0.826	0.048	0.903	0.955	0.856	0.016

4.2 Implementation Details

All experiments are implemented in PyTorch on an NVIDIA A100 GPU. We follow a similar training setting as [0, 8] with an image size of 1024×1024 . We use pre-trained SAM and SAM2 networks as the backbone.

4.3 Experimental Results

Camouflaged Object Detection: We compare our approach with existing task-specific methods [36, 41, 45] and efficient tuning methods [2, 37]. Tab. 2 shows that SAMwave significantly outperforms these methods across three datasets, consistently with both SAM and SAM2 backbones. To demonstrate the efficacy of our adaptive approach, we show that performance improvement over previous methods is consistent across different wavelets. Despite vanilla SAM2 performing poorly compared to SAM and other methods in Tab. 2, its performance is significantly boosted when combined with our approach. Qualitative results are provided in Fig. 4.

Table 3: Comparison of state-of-the-art approaches on shadow detection. (■: best, ■: second best)







Dataset	DSD ()	FDRNet ()	MTMT ()	EVP ()	SAM- Adapter()	SAM2- Adapter()	Ours											
							SAM as Backbone						SAM2 as Backbone					
							Real-valued Adapters			Complex-valued Adapters			Real-valued Adapters			Complex-valued Adapters		
							db	cf	ha	sym	sy-b	sy-a	db	cf	ha	sym	sy-b	sy-a
ISTD (BER _L)	2.17	1.55	1.72	1.35	1.43	1.43	1.24	1.24	1.01	1.04	1.09	1.15	1.91	1.24	0.92	1.22	2.60	1.32
SBU (BER _L)	3.45	3.04	3.15	4.31	-	-	2.93	3.01	3.00	3.07	3.06	3.06	3.04	5.28	2.99	3.77	4.43	4.32



Figure 4: Visual comparison of our proposed SAMwave with existing methods for the COD task.

Shadow Detection: We compare the performance of our approach against existing methods across two benchmark datasets. In both cases, our method yields substantial performance improvements. Although the performance improvements are relatively smaller on the ISTD dataset when using Daubechies and Coiflet wavelets compared to other wavelet variants, the improvement remains significant, demonstrating the robustness and generalizability of our adaptive approach.

Table 4: Comparison with state-of-the-art approaches on blur detection. (■: best, ■: second best)





Dataset		DeFusion-Net	BTBNet	CENet	DAD	EFENet	EVP	Ours											
								SAM as Backbone						SAM2 as Backbone					
								Real-valued Adapters				Complex-valued Adapters		Real-valued Adapters				Complex-valued Adapters	
								db	cf	ha	sym	sy-b	sy-a	db	cf	ha	sym	sy-b	sy-a
DUT	$\mathcal{F}_\beta \uparrow$	0.823	0.827	0.817	0.794	0.854	0.890	0.888	0.886	0.880	0.885	0.892	0.893	0.896	0.893	0.894	0.893	0.907	0.902
	$\mathcal{M} \downarrow$	0.118	0.138	0.135	0.153	0.094	0.068	0.068	0.067	0.108	0.106	0.067	0.066	0.051	0.051	0.051	0.051	0.052	0.056
CHUK	$\mathcal{F}_\beta \uparrow$	0.818	0.889	0.906	0.884	0.914	0.928	0.922	0.916	0.911	0.911	0.917	0.912	0.923	0.924	0.925	0.924	0.928	0.925
	$\mathcal{M} \downarrow$	0.117	0.082	0.059	0.079	0.053	0.045	0.040	0.046	0.070	0.069	0.045	0.046	0.036	0.039	0.037	0.038	0.036	0.039

Defocus Blur Detection: For the Blur Detection task, we primarily compare our method with EVP[57], as SAM-Adapter[4] does not report results for this task. As shown in Tab. 4, our approach achieves the best results when using complex-valued adapters with the SAM2 backbone. While we outperform EVP in all cases, our method demonstrates significant improvements over other existing approaches as well.

PolyP Detection: Tab. 5 presents quantitative results for the PolyP detection task. Compared to existing approaches[4, 8, 57, 58], our method achieves significant improvements across nearly all datasets. Notably, we observe further gains when using the SAM2 backbone, especially in conjunction with complex-valued adapters. While our performance is comparable to that of [58], it is important to emphasize that—unlike their task-specific model—our adaptive approach is designed to generalize across multiple low-level vision tasks.

R-valued vs C-valued Adapters: Tab. 2, 3, 4, and 5 show that, when using the SAM backbone, complex-valued adapters perform comparably to—or in some cases better than—their real-valued adapters. Furthermore, when switching to the SAM2 backbone, complex-valued adapters consistently yield improved results, highlighting the enhanced compatibility and

Table 5: Comparison with state-of-the-art methods on PolyP detection. (■: best, ■: second best)

Dataset		M ² UNet 	SAM Adapter 	SAM2 Adapter 	SAM-EG 	Ours											
						SAM as Backbone						SAM2 as Backbone					
						Real-valued Adapters				Complex-valued Adapters		Real-valued Adapters				Complex-valued Adapters	
						db	cf	ha	sym	sy-b	sy-a	db	cf	ha	sym	sy-b	sy-a
ClinicDB	mDice↑	0.901	-	-	0.931	0.855	0.652	0.866	0.854	0.832	0.840	0.887	0.881	0.885	0.874	0.862	0.846
	mIoU↑	0.853	-	-	0.879	0.789	0.449	0.794	0.786	0.761	0.772	0.826	0.821	0.827	0.816	0.800	0.784
ColonDB	mDice↑	0.767	-	-	0.774	0.743	0.635	0.724	0.737	0.726	0.748	0.764	0.769	0.769	0.778	0.781	0.782
	mIoU↑	0.684	-	-	0.689	0.668	0.386	0.647	0.661	0.652	0.671	0.696	0.703	0.697	0.704	0.710	0.707
Kvasir	mDice↑	0.907	0.850	0.873	0.915	0.889	0.812	0.901	0.900	0.901	0.902	0.917	0.913	0.911	0.908	0.899	0.902
	mIoU↑	0.855	0.776	0.806	0.862	0.818	0.618	0.827	0.828	0.834	0.838	0.867	0.861	0.859	0.860	0.844	0.847
ETIS	mDice↑	0.670	-	-	0.757	0.688	0.445	0.685	0.693	0.680	0.732	0.780	0.749	0.784	0.802	0.797	0.750
	mIoU↑	0.595	-	-	0.681	0.610	0.223	0.603	0.622	0.611	0.654	0.709	0.683	0.720	0.737	0.730	0.676

representational capacity of SAM2 for this task.

Table 6: The results of our ablation study highlight the importance of adapters for efficient finetuning; it also highlights the importance of each low-frequency subband (*LL*) and the rest of the high-frequency subbands (*HL*, *LH*, *HH*) in the image in the wavelet domain. The ablation experiment is done for camouflage object detection, and SAM is taken as the backbone.

Method					CHAMELEON					CAMO					COD10K				
					$S_m \uparrow$	$\mathcal{E}_\phi \uparrow$	$\mathcal{F}_B^w \uparrow$	$\mathcal{M} \downarrow$		$S_m \uparrow$	$\mathcal{E}_\phi \uparrow$	$\mathcal{F}_B^w \uparrow$	$\mathcal{M} \downarrow$		$S_m \uparrow$	$\mathcal{E}_\phi \uparrow$	$\mathcal{F}_B^w \uparrow$	$\mathcal{M} \downarrow$	
SAM Finetuned					0.796	0.802	0.676	0.062		0.750	0.756	0.639	0.105		0.789	0.817	0.596	0.049	
<i>LL</i> <i>HL</i> <i>LH</i> <i>HH</i>					Evaluating each component														
✓	✓	✓	✓	✓	0.907	0.937	0.842	0.029		0.856	0.884	0.785	0.062		0.891	0.929	0.817	0.024	
✓	✓	✓	✓	✓	0.895	0.927	0.834	0.030		0.851	0.882	0.781	0.063		0.887	0.924	0.816	0.024	
✓	✓	✓	✓	✓	0.896	0.915	0.838	0.030		0.854	0.887	0.790	0.063		0.891	0.928	0.838	0.023	
✓	✓	✓	✓	✓	0.908	0.935	0.848	0.028		0.853	0.883	0.783	0.064		0.893	0.928	0.818	0.023	
✓	✓	✓	✓	✓	0.923	0.952	0.890	0.022		0.856	0.888	0.807	0.060		0.903	0.939	0.857	0.019	

4.4 Ablation Study

We conduct three ablation studies to highlight our contribution. First, we remove the WHF module and adapters from the SAM backbone while keeping everything else the same, and then we provide each of the subbands of wavelets transform. Lastly, we replace the wavelets used in our approach with other wavelets and observe the result.

Effect of adapters: We remove high-frequency features and patch embeddings from the backbone and train the SAM model. Tab. 6 shows the result for the same. Although this helped improve performance over SAM, it lags significantly.

Effect of each subband: In §3.3, we claim that when combining all three high-frequency subbands (*HL*, *LH*, *HH*), there is a significant improvement in the performance. Hence, we perform an ablation study by considering each subband individually and observing their significance to assert our claim. As expected, when provided with low-frequency features (*LL*), we see performance degradation for all three datasets. Similarly, when we provide each high-frequency subband, we see a similar pattern in performance loss. However, we only see the best performance when all three are combined.

Effect of each wavelet: To ensure that the results obtained are not due to any specific property of a single wavelet, we use four different wavelets and show their results. The comparative result are shown in Tab. 2, 3, 4, 5. The observation is similar across all four tasks; we see more performance gain for some wavelets, but overall, using any wavelet provides better finer detail information than previous methods.

5 Conclusion

This work presents a new efficient fine-tuning method for large vision models, particularly SAM and SAM2, for solving four different low-level vision tasks. Additionally, we show that a complex-valued adapter can be used to fine-tune large vision models efficiently. We first show that the existing method of providing high-frequency information to the network is not optimal and needs improvement. We propose a WHF module, which converts the input image to a wavelet domain and combines the high-frequency subbands. When provided to the networks, this new feature map shows significant improvement over existing methods.

References

- [1] Sara Babakniya, Zalan Fabian, Chaoyang He, Mahdi Soltanolkotabi, and Salman Avestimehr. A data-free approach to mitigate catastrophic forgetting in federated class incremental learning for vision tasks. In Alice Oh, Tristan Naumann, Amir Globerson, Kate Saenko, Moritz Hardt, and Sergey Levine, editors, *Advances in Neural Information Processing Systems 36: Annual Conference on Neural Information Processing Systems 2023, NeurIPS 2023, New Orleans, LA, USA, December 10 - 16, 2023*, 2023. URL http://papers.nips.cc/paper_files/paper/2023/hash/d160ea01902c33e30660851dfbac5980-Abstract-Conference.html.
- [2] Jorge Bernal, Francisco Javier Sánchez, Gloria Fernández-Esparrach, Debora Gil, Cristina Rodríguez de Miguel, and Fernando Vilariño. WM-DOVA maps for accurate polyp highlighting in colonoscopy: Validation vs. saliency maps from physicians. *Comput. Medical Imaging Graph.*, 43:99–111, 2015. doi: 10.1016/J.COMPAMEDIMAG.2015.02.007. URL <https://doi.org/10.1016/j.compmedimag.2015.02.007>.
- [3] David Brüggemann, Menelaos Kanakis, Anton Obukhov, Stamatios Georgoulis, and Luc Van Gool. Exploring relational context for multi-task dense prediction. In *2021 IEEE/CVF International Conference on Computer Vision, ICCV 2021, Montreal, QC, Canada, October 10-17, 2021*, pages 15849–15858. IEEE, 2021. doi: 10.1109/ICCV48922.2021.01557. URL <https://doi.org/10.1109/ICCV48922.2021.01557>.
- [4] Xinzi Cao, Xiwu Zheng, Guanhong Wang, Weijiang Yu, Yunhang Shen, Ke Li, Yutong Lu, and Yonghong Tian. Solving the catastrophic forgetting problem in generalized category discovery. In *Proceedings of the IEEE/CVF Conference on Computer Vision and Pattern Recognition (CVPR)*, pages 16880–16889, June 2024.
- [5] Nicolas Carion, Francisco Massa, Gabriel Synnaeve, Nicolas Usunier, Alexander Kirillov, and Sergey Zagoruyko. End-to-end object detection with transformers. In Andrea Vedaldi, Horst Bischof, Thomas Brox, and Jan-Michael Frahm, editors, *Computer Vision - ECCV 2020 - 16th European Conference, Glasgow, UK, August 23-28, 2020, Proceedings, Part I*, volume 12346 of *Lecture Notes in Computer Science*, pages 213–229. Springer, 2020. doi: 10.1007/978-3-030-58452-8_13. URL https://doi.org/10.1007/978-3-030-58452-8_13.

- [6] Jinpeng Chen, Runmin Cong, Yuxuan Luo, Horace Ho-Shing Ip, and Sam Kwong. Saving 100x storage: Prototype replay for reconstructing training sample distribution in class-incremental semantic segmentation. In Alice Oh, Tristan Naumann, Amir Globerson, Kate Saenko, Moritz Hardt, and Sergey Levine, editors, *Advances in Neural Information Processing Systems 36: Annual Conference on Neural Information Processing Systems 2023, NeurIPS 2023, New Orleans, LA, USA, December 10 - 16, 2023*, 2023. URL http://papers.nips.cc/paper_files/paper/2023/hash/708e0d691a22212e1e373dc8779cbe53-Abstract-Conference.html.
- [7] Tianrun Chen, Lanyun Zhu, Chaotao Ding, Runlong Cao, Shangzhan Zhang, Yan Wang, Zejian Li, Lingyun Sun, Papa Mao, and Ying Zang. Sam fails to segment anything? – sam-adapter: Adapting sam in underperformed scenes: Camouflage, shadow, and more, 2023.
- [8] Tianrun Chen, Ankang Lu, Lanyun Zhu, Chaotao Ding, Chunan Yu, Deyi Ji, Zejian Li, Lingyun Sun, Papa Mao, and Ying Zang. Sam2-adapter: Evaluating & adapting segment anything 2 in downstream tasks: Camouflage, shadow, medical image segmentation, and more, 2024. URL <https://arxiv.org/abs/2408.04579>.
- [9] Zhe Chen, Yuchen Duan, Wenhai Wang, Junjun He, Tong Lu, Jifeng Dai, and Yu Qiao. Vision transformer adapter for dense predictions. In *The Eleventh International Conference on Learning Representations, ICLR 2023, Kigali, Rwanda, May 1-5, 2023*. OpenReview.net, 2023. URL <https://openreview.net/pdf?id=plKu2GByCNW>.
- [10] Zhihao Chen, Lei Zhu, Liang Wan, Song Wang, Wei Feng, and Pheng-Ann Heng. A multi-task mean teacher for semi-supervised shadow detection. In *2020 IEEE/CVF Conference on Computer Vision and Pattern Recognition, CVPR 2020, Seattle, WA, USA, June 13-19, 2020*, pages 5610–5619. Computer Vision Foundation / IEEE, 2020. doi: 10.1109/CVPR42600.2020.00565. URL https://openaccess.thecvf.com/content_CVPR_2020/html/Chen_A_Multi-Task_Mean_Teacher_for_Semi-Supervised_Shadow_Detection_CVPR_2020_paper.html.
- [11] Bowen Cheng, Alexander G. Schwing, and Alexander Kirillov. Per-pixel classification is not all you need for semantic segmentation. 2021.
- [12] Xiaodong Cun and Chi-Man Pun. Image splicing localization via semi-global network and fully connected conditional random fields. In Laura Leal-Taixé and Stefan Roth, editors, *Computer Vision - ECCV 2018 Workshops - Munich, Germany, September 8-14, 2018, Proceedings, Part II*, volume 11130 of *Lecture Notes in Computer Science*, pages 252–266. Springer, 2018. doi: 10.1007/978-3-030-11012-3_22. URL https://doi.org/10.1007/978-3-030-11012-3_22.
- [13] Pieter-Tjerk de Boer, Dirk P. Kroese, Shie Mannor, and Reuven Y. Rubinstein. A tutorial on the cross-entropy method. *Ann. Oper. Res.*, 134(1):19–67, 2005. doi: 10.1007/S10479-005-5724-Z. URL <https://doi.org/10.1007/s10479-005-5724-z>.
- [14] Jing Dong, Wei Wang, and Tieniu Tan. Casia image tampering detection evaluation database. In *2013 IEEE China Summit and International Conference on Signal and Information Processing*, pages 422–426, 2013. doi: 10.1109/ChinaSIP.2013.6625374.

- [15] Alexey Dosovitskiy, Lucas Beyer, Alexander Kolesnikov, Dirk Weissenborn, Xiaohua Zhai, Thomas Unterthiner, Mostafa Dehghani, Matthias Minderer, Georg Heigold, Sylvain Gelly, Jakob Uszkoreit, and Neil Houlsby. An image is worth 16x16 words: Transformers for image recognition at scale. In *9th International Conference on Learning Representations, ICLR 2021, Virtual Event, Austria, May 3-7, 2021*. OpenReview.net, 2021. URL <https://openreview.net/forum?id=YicbFdNTTy>.
- [16] Deng-Ping Fan, Ming-Ming Cheng, Yun Liu, Tao Li, and Ali Borji. Structure-measure: A new way to evaluate foreground maps. In *Proceedings of the IEEE International Conference on Computer Vision (ICCV)*, Oct 2017.
- [17] Deng-Ping Fan, Ge-Peng Ji, Guolei Sun, Ming-Ming Cheng, Jianbing Shen, and Ling Shao. Camouflaged object detection. In *IEEE/CVF Conference on Computer Vision and Pattern Recognition (CVPR)*, June 2020.
- [18] Jessica J. Fridrich and Jan Kodovský. Rich models for steganalysis of digital images. *IEEE Trans. Inf. Forensics Secur.*, 7(3):868–882, 2012. doi: 10.1109/TIFS.2012.2190402. URL <https://doi.org/10.1109/TIFS.2012.2190402>.
- [19] Avi Gupta, Koteswar Rao Jerripothula, and Tammam Tillo. CIRCOC: co-saliency inspired referring camouflaged object discovery. In *IEEE/CVF Winter Conference on Applications of Computer Vision, WACV 2025, Tucson, AZ, USA, February 26 - March 6, 2025*, pages 8313–8323. IEEE, 2025. doi: 10.1109/WACV61041.2025.00806. URL <https://doi.org/10.1109/WACV61041.2025.00806>.
- [20] Jing Hao, Zhixin Zhang, Shicai Yang, Di Xie, and Shiliang Pu. Transforensics: Image forgery localization with dense self-attention. In *2021 IEEE/CVF International Conference on Computer Vision, ICCV 2021, Montreal, QC, Canada, October 10-17, 2021*, pages 15035–15044. IEEE, 2021. doi: 10.1109/ICCV48922.2021.01478. URL <https://doi.org/10.1109/ICCV48922.2021.01478>.
- [21] Alvin Heng and Harold Soh. Selective amnesia: A continual learning approach to forgetting in deep generative models. In Alice Oh, Tristan Naumann, Amir Globerson, Kate Saenko, Moritz Hardt, and Sergey Levine, editors, *Advances in Neural Information Processing Systems 36: Annual Conference on Neural Information Processing Systems 2023, NeurIPS 2023, New Orleans, LA, USA, December 10 - 16, 2023*, 2023. URL http://papers.nips.cc/paper_files/paper/2023/hash/376276a95781fa17c177b1ccdd0a03ac-Abstract-Conference.html.
- [22] Neil Houlsby, Andrei Giurgiu, Stanislaw Jastrzebski, Bruna Morrone, Quentin de Laroussilhe, Andrea Gesmundo, Mona Attariyan, and Sylvain Gelly. Parameter-efficient transfer learning for NLP. In Kamalika Chaudhuri and Ruslan Salakhutdinov, editors, *Proceedings of the 36th International Conference on Machine Learning, ICML 2019, 9-15 June 2019, Long Beach, California, USA*, volume 97 of *Proceedings of Machine Learning Research*, pages 2790–2799. PMLR, 2019. URL <http://proceedings.mlr.press/v97/houlsby19a.html>.
- [23] Xiaowei Hu, Lei Zhu, Chi-Wing Fu, Jing Qin, and Pheng-Ann Heng. Direction-aware spatial context features for shadow detection. In *2018 IEEE Conference on Computer Vision and Pattern Recognition, CVPR 2018, Salt Lake*

- City, UT, USA, June 18-22, 2018, pages 7454–7462. Computer Vision Foundation / IEEE Computer Society, 2018. doi: 10.1109/CVPR.2018.00778. URL http://openaccess.thecvf.com/content_cvpr_2018/html/Hu_Direction-Aware_Spatial_Context_CVPR_2018_paper.html.
- [24] Xuefeng Hu, Zhihan Zhang, Zhenye Jiang, Syomantak Chaudhuri, Zhenheng Yang, and Ram Nevatia. SPAN: spatial pyramid attention network for image manipulation localization. In Andrea Vedaldi, Horst Bischof, Thomas Brox, and Jan-Michael Frahm, editors, *Computer Vision - ECCV 2020 - 16th European Conference, Glasgow, UK, August 23-28, 2020, Proceedings, Part XXI*, volume 12366 of *Lecture Notes in Computer Science*, pages 312–328. Springer, 2020. doi: 10.1007/978-3-030-58589-1_19. URL https://doi.org/10.1007/978-3-030-58589-1_19.
- [25] Zhou Huang, Hang Dai, Tian-Zhu Xiang, Shuo Wang, Huai-Xin Chen, Jie Qin, and Huan Xiong. Feature shrinkage pyramid for camouflaged object detection with transformers. In *IEEE/CVF Conference on Computer Vision and Pattern Recognition, CVPR 2023, Vancouver, BC, Canada, June 17-24, 2023*, pages 5557–5566. IEEE, 2023. doi: 10.1109/CVPR52729.2023.00538. URL <https://doi.org/10.1109/CVPR52729.2023.00538>.
- [26] Debesh Jha, Pia H. Smedsrud, Michael A. Riegler, Pål Halvorsen, Thomas de Lange, Dag Johansen, and Håvard D. Johansen. Kvasir-seg: A segmented polyp dataset. In Yong Man Ro, Wen-Huang Cheng, Junmo Kim, Wei-Ta Chu, Peng Cui, Jung-Woo Choi, Min-Chun Hu, and Wesley De Neve, editors, *MultiMedia Modeling - 26th International Conference, MMM 2020, Daejeon, South Korea, January 5-8, 2020, Proceedings, Part II*, volume 11962 of *Lecture Notes in Computer Science*, pages 451–462. Springer, 2020. doi: 10.1007/978-3-030-37734-2_37. URL https://doi.org/10.1007/978-3-030-37734-2_37.
- [27] Ali Karaali and Cláudio R. Jung. Edge-based defocus blur estimation with adaptive scale selection. *IEEE Trans. Image Process.*, 27(3):1126–1137, 2018. doi: 10.1109/TIP.2017.2771563. URL <https://doi.org/10.1109/TIP.2017.2771563>.
- [28] Alexander Kirillov, Eric Mintun, Nikhila Ravi, Hanzi Mao, Chloé Rolland, Laura Gustafson, Tete Xiao, Spencer Whitehead, Alexander C. Berg, Wan-Yen Lo, Piotr Dollár, and Ross B. Girshick. Segment anything. In *IEEE/CVF International Conference on Computer Vision, ICCV 2023, Paris, France, October 1-6, 2023*, pages 3992–4003. IEEE, 2023. doi: 10.1109/ICCV51070.2023.00371. URL <https://doi.org/10.1109/ICCV51070.2023.00371>.
- [29] Cansu Korkmaz, A. Murat Tekalp, and Zafer Dogan. Training generative image super-resolution models by wavelet-domain losses enables better control of artifacts. *CoRR*, abs/2402.19215, 2024. doi: 10.48550/ARXIV.2402.19215. URL <https://doi.org/10.48550/arXiv.2402.19215>.
- [30] Trung-Nghia Le, Tam V. Nguyen, Zhongliang Nie, Minh-Triet Tran, and Akihiro Sugimoto. Anabran network for camouflaged object segmentation. *Journal of Computer Vision and Image Understanding*, 184:45–56, 2019.

- [31] Aixuan Li, Jing Zhang, Yunqiu Lv, Bowen Liu, Tong Zhang, and Yuchao Dai. Uncertainty-aware joint salient object and camouflaged object detection. In *IEEE Conference on Computer Vision and Pattern Recognition, CVPR 2021, virtual, June 19-25, 2021*, pages 10071–10081. Computer Vision Foundation / IEEE, 2021. doi: 10.1109/CVPR46437.2021.00994. URL https://openaccess.thecvf.com/content/CVPR2021/html/Li_Uncertainty-Aware-Joint-Salient-Object_and_Camouflaged-Object-Detection_CVPR_2021_paper.html.
- [32] Aixuan Li, Jing Zhang, Yunqiu Lyu, Bowen Liu, Tong Zhang, and Yuchao Dai. Uncertainty-aware joint salient object and camouflaged object detection. In *Proceedings of the IEEE/CVF Conference on Computer Vision and Pattern Recognition (CVPR)*, 2021.
- [33] Jin Li, Yaoming Wang, Xiaopeng Zhang, Bowen Shi, Dongsheng Jiang, Chenglin Li, Wenrui Dai, Hongkai Xiong, and Qi Tian. Ailurus: A scalable vit framework for dense prediction. In Alice Oh, Tristan Naumann, Amir Globerson, Kate Saenko, Moritz Hardt, and Sergey Levine, editors, *Advances in Neural Information Processing Systems 36: Annual Conference on Neural Information Processing Systems 2023, NeurIPS 2023, New Orleans, LA, USA, December 10 - 16, 2023*, 2023. URL http://papers.nips.cc/paper_files/paper/2023/hash/62c9aa4d48329a85d1e36d5b6d0a6a32-Abstract-Conference.html.
- [34] Wei-Hong Li, Xialei Liu, and Hakan Bilen. Learning multiple dense prediction tasks from partially annotated data. In *IEEE/CVF Conference on Computer Vision and Pattern Recognition, CVPR 2022, New Orleans, LA, USA, June 18-24, 2022*, pages 18857–18867. IEEE, 2022. doi: 10.1109/CVPR52688.2022.01831. URL <https://doi.org/10.1109/CVPR52688.2022.01831>.
- [35] Yanghao Li, Hanzi Mao, Ross B. Girshick, and Kaiming He. Exploring plain vision transformer backbones for object detection. In Shai Avidan, Gabriel J. Brostow, Moustapha Cissé, Giovanni Maria Farinella, and Tal Hassner, editors, *Computer Vision - ECCV 2022 - 17th European Conference, Tel Aviv, Israel, October 23-27, 2022, Proceedings, Part IX*, volume 13669 of *Lecture Notes in Computer Science*, pages 280–296. Springer, 2022. doi: 10.1007/978-3-031-20077-9_17. URL https://doi.org/10.1007/978-3-031-20077-9_17.
- [36] Jiaying Lin, Xin Tan, Ke Xu, Lizhuang Ma, and Rynson W. H. Lau. Frequency-aware camouflaged object detection. *ACM Trans. Multim. Comput. Commun. Appl.*, 19(2): 61:1–61:16, 2023. doi: 10.1145/3545609. URL <https://doi.org/10.1145/3545609>.
- [37] Weihuang Liu, Xi Shen, Chi-Man Pun, and Xiaodong Cun. Explicit visual prompting for low-level structure segmentations. In *IEEE/CVF Conference on Computer Vision and Pattern Recognition, CVPR 2023, Vancouver, BC, Canada, June 17-24, 2023*, pages 19434–19445. IEEE, 2023. doi: 10.1109/CVPR52729.2023.01862. URL <https://doi.org/10.1109/CVPR52729.2023.01862>.
- [38] Xiaohong Liu, Yaojie Liu, Jun Chen, and Xiaoming Liu. Pscn-net: Progressive spatio-channel correlation network for image manipulation detection and localization. *IEEE Transactions on Circuits and Systems for Video Technology*, 2022.

- [39] Ange Lou, Benjamin Planche, Zhongpai Gao, Yamin Li, Tianyu Luan, Hao Ding, Terrence Chen, Jack Noble, and Ziyang Wu. Darenerf: Direction-aware representation for dynamic scenes. In *Proceedings of the IEEE/CVF Conference on Computer Vision and Pattern Recognition (CVPR)*, pages 5031–5042, June 2024.
- [40] Yuxiang Lu, Shalayiding Sirejiding, Yue Ding, Chunlin Wang, and Hongtao Lu. Prompt guided transformer for multi-task dense prediction. *IEEE Trans. Multimed.*, 26: 6375–6385, 2024. doi: 10.1109/TMM.2024.3349865. URL <https://doi.org/10.1109/TMM.2024.3349865>.
- [41] Yunqiu Lv, Jing Zhang, Yuchao Dai, Aixuan Li, Bowen Liu, Nick Barnes, and Deng-Ping Fan. Simultaneously localize, segment and rank the camouflaged objects. In *IEEE Conference on Computer Vision and Pattern Recognition, CVPR 2021, virtual, June 19-25, 2021*, pages 11591–11601. Computer Vision Foundation / IEEE, 2021. doi: 10.1109/CVPR46437.2021.01142. URL https://openaccess.thecvf.com/content/CVPR2021/html/Lv_Simultaneously_Localize_Segment_and_Rank_the_Camouflaged_Objects_CVPR_2021_paper.html.
- [42] Yunqiu Lyu, Jing Zhang, Yuchao Dai, Aixuan Li, Bowen Liu, Nick Barnes, and Deng-Ping Fan. Simultaneously localize, segment and rank the camouflaged objects. In *Proceedings of the IEEE/CVF Conference on Computer Vision and Pattern Recognition (CVPR)*, 2021.
- [43] Ran Margolin, Lihi Zelnik-Manor, and Ayellet Tal. How to evaluate foreground maps? In *Proceedings of the IEEE Conference on Computer Vision and Pattern Recognition (CVPR)*, June 2014.
- [44] Haiyang Mei, Ge-Peng Ji, Ziqi Wei, Xin Yang, Xiaopeng Wei, and Deng-Ping Fan. Camouflaged object segmentation with distraction mining. In *IEEE Conference on Computer Vision and Pattern Recognition, CVPR 2021, virtual, June 19-25, 2021*, pages 8772–8781. Computer Vision Foundation / IEEE, 2021. doi: 10.1109/CVPR46437.2021.00866. URL https://openaccess.thecvf.com/content/CVPR2021/html/Mei_Camouflaged_Object_Segmentation_With_Distraction_Mining_CVPR_2021_paper.html.
- [45] Haiyang Mei, Ge-Peng Ji, Ziqi Wei, Xin Yang, Xiaopeng Wei, and Deng-Ping Fan. Camouflaged object segmentation with distraction mining. In *Proceedings of the IEEE/CVF Conference on Computer Vision and Pattern Recognition (CVPR)*, pages 8772–8781, June 2021.
- [46] Adam Novozámský, Babak Mahdian, and Stanislav Saic. Imd2020: A large-scale annotated dataset tailored for detecting manipulated images. In *2020 IEEE Winter Applications of Computer Vision Workshops (WACVW)*, pages 71–80, 2020. doi: 10.1109/WACVW50321.2020.9096940.
- [47] Maxime Oquab, Timothée Darcet, Théo Moutakanni, Huy V. Vo, Marc Szafraniec, Vasil Khalidov, Pierre Fernandez, Daniel Haziza, Francisco Massa, Alaaeldin El-Nouby, Mido Assran, Nicolas Ballas, Wojciech Galuba, Russell Howes, Po-Yao Huang, Shang-Wen Li, Ishan Misra, Michael Rabbat, Vasu Sharma, Gabriel Synnaeve, Hu Xu, Hervé Jégou, Julien Mairal, Patrick Labatut, Armand Joulin, and Piotr Bojanowski. Dinov2: Learning robust visual features without supervision. *Trans.*

- Mach. Learn. Res.*, 2024, 2024. URL <https://openreview.net/forum?id=a68SUt6zFt>.
- [48] Youwei Pang, Xiaoqi Zhao, Tian-Zhu Xiang, Lihe Zhang, and Huchuan Lu. Zoom in and out: A mixed-scale triplet network for camouflaged object detection. In *Proceedings of the IEEE/CVF Conference on Computer Vision and Pattern Recognition (CVPR)*, pages 2160–2170, June 2022.
- [49] Alec Radford, Jong Wook Kim, Chris Hallacy, Aditya Ramesh, Gabriel Goh, Sandhini Agarwal, Girish Sastry, Amanda Askell, Pamela Mishkin, Jack Clark, Gretchen Krueger, and Ilya Sutskever. Learning transferable visual models from natural language supervision. In Marina Meila and Tong Zhang, editors, *Proceedings of the 38th International Conference on Machine Learning, ICML 2021, 18-24 July 2021, Virtual Event*, volume 139 of *Proceedings of Machine Learning Research*, pages 8748–8763. PMLR, 2021. URL <http://proceedings.mlr.press/v139/radford21a.html>.
- [50] Michaël Ramamonjisoa, Michael Firman, Jamie Watson, Vincent Lepetit, and Daniyar Turmukhambetov. Single image depth prediction with wavelet decomposition. In *IEEE Conference on Computer Vision and Pattern Recognition, CVPR 2021, virtual, June 19-25, 2021*, pages 11089–11098. Computer Vision Foundation / IEEE, 2021. doi: 10.1109/CVPR46437.2021.01094. URL https://openaccess.thecvf.com/content/CVPR2021/html/Ramamonjisoa_Single_Image_Depth_Prediction_With_Wavelet_Decomposition_CVPR_2021_paper.html.
- [51] René Ranftl, Alexey Bochkovskiy, and Vladlen Koltun. Vision transformers for dense prediction. In *2021 IEEE/CVF International Conference on Computer Vision, ICCV 2021, Montreal, QC, Canada, October 10-17, 2021*, pages 12159–12168. IEEE, 2021. doi: 10.1109/ICCV48922.2021.01196. URL <https://doi.org/10.1109/ICCV48922.2021.01196>.
- [52] Nikhila Ravi, Valentin Gabeur, Yuan-Ting Hu, Ronghang Hu, Chaitanya Ryali, Tengyu Ma, Haitham Khedr, Roman Rädle, Chloe Rolland, Laura Gustafson, Eric Mintun, Junting Pan, Kalyan Vasudev Alwala, Nicolas Carion, Chao-Yuan Wu, Ross Girshick, Piotr Dollár, and Christoph Feichtenhofer. Sam 2: Segment anything in images and videos. *arXiv preprint arXiv:2408.00714*, 2024. URL <https://arxiv.org/abs/2408.00714>.
- [53] Nikhila Ravi, Valentin Gabeur, Yuan-Ting Hu, Ronghang Hu, Chaitanya Ryali, Tengyu Ma, Haitham Khedr, Roman Rädle, Chloé Rolland, Laura Gustafson, Eric Mintun, Junting Pan, Kalyan Vasudev Alwala, Nicolas Carion, Chao-Yuan Wu, Ross B. Girshick, Piotr Dollár, and Christoph Feichtenhofer. SAM 2: Segment anything in images and videos. In *The Thirteenth International Conference on Learning Representations, ICLR 2025, Singapore, April 24-28, 2025*. OpenReview.net, 2025. URL <https://openreview.net/forum?id=Ha6RTeWMd0>.
- [54] Vishwanath Saragadam, Daniel LeJeune, Jasper Tan, Guha Balakrishnan, Ashok Veeraghavan, and Richard G. Baraniuk. Wire: Wavelet implicit neural representations. In *Proceedings of the IEEE/CVF Conference on Computer Vision and Pattern Recognition (CVPR)*, pages 18507–18516, June 2023.

- [55] Vanshali Sharma, Abhishek Kumar, Debesh Jha, Manas Kamal Bhuyan, Pradip K. Das, and Ulas Bagci. Controlpolypnet: Towards controlled colon polyp synthesis for improved polyp segmentation. In *IEEE/CVF Conference on Computer Vision and Pattern Recognition, CVPR 2024 - Workshops, Seattle, WA, USA, June 17-18, 2024*, pages 2325–2334. IEEE, 2024. doi: 10.1109/CVPRW63382.2024.00238. URL <https://doi.org/10.1109/CVPRW63382.2024.00238>.
- [56] Jianping Shi, Li Xu, and Jiaya Jia. Discriminative blur detection features. In *2014 IEEE Conference on Computer Vision and Pattern Recognition, CVPR 2014, Columbus, OH, USA, June 23-28, 2014*, pages 2965–2972. IEEE Computer Society, 2014. doi: 10.1109/CVPR.2014.379. URL <https://doi.org/10.1109/CVPR.2014.379>.
- [57] Jianping Shi, Li Xu, and Jiaya Jia. Just noticeable defocus blur detection and estimation. In *IEEE Conference on Computer Vision and Pattern Recognition, CVPR 2015, Boston, MA, USA, June 7-12, 2015*, pages 657–665. IEEE Computer Society, 2015. doi: 10.1109/CVPR.2015.7298665. URL <https://doi.org/10.1109/CVPR.2015.7298665>.
- [58] Hanul Shin, Jung Kwon Lee, Jaehong Kim, and Jiwon Kim. Continual learning with deep generative replay. In Isabelle Guyon, Ulrike von Luxburg, Samy Bengio, Hanna M. Wallach, Rob Fergus, S. V. N. Vishwanathan, and Roman Garnett, editors, *Advances in Neural Information Processing Systems 30: Annual Conference on Neural Information Processing Systems 2017, December 4-9, 2017, Long Beach, CA, USA*, pages 2990–2999, 2017. URL <https://proceedings.neurips.cc/paper/2017/hash/0efbe98067c6c73dba1250d2beaa81f9-Abstract.html>.
- [59] Juan Silva, Aymeric Histace, Olivier Romain, Xavier Dray, and Bertrand Granado. Toward embedded detection of polyps in wce images for early diagnosis of colorectal cancer. *International journal of computer assisted radiology and surgery*, 9(2):283–293, March 2014. ISSN 1861-6410. doi: 10.1007/s11548-013-0926-3. URL https://hal.archives-ouvertes.fr/hal-00843459/file/IJCARS_R2_vf.pdf.
- [60] Przemysław Skurowski, Hassan Abdulameer, J Błaszczyk, Tomasz Depta, Adam Kornacki, and P Kozieł. Animal camouflage analysis: Chameleon database. *Unpublished manuscript*, 2(6):7, 2018.
- [61] Xiang Song, Kuang Shu, Songlin Dong, Jie Cheng, Xing Wei, and Yihong Gong. Overcoming catastrophic forgetting for multi-label class-incremental learning. In *IEEE/CVF Winter Conference on Applications of Computer Vision, WACV 2024, Waikoloa, HI, USA, January 3-8, 2024*, pages 2378–2387. IEEE, 2024. doi: 10.1109/WACV57701.2024.00238. URL <https://doi.org/10.1109/WACV57701.2024.00238>.
- [62] Gilbert Strang and Truong Q. Nguyen. *Wavelets and filter banks*. Wellesley-Cambridge Press, 1997. ISBN 978-0-9614088-7-9.
- [63] Nima Tajbakhsh, Suryakanth R. Gurudu, and Jianming Liang. Automated polyp detection in colonoscopy videos using shape and context information. *IEEE Trans. Medical Imaging*, 35(2):630–644, 2016. doi: 10.1109/TMI.2015.2487997. URL <https://doi.org/10.1109/TMI.2015.2487997>.

- [64] Chang Tang, Xinzhong Zhu, Xinwang Liu, Lizhe Wang, and Albert Y. Zomaya. Defusionnet: Defocus blur detection via recurrently fusing and refining multi-scale deep features. In *IEEE Conference on Computer Vision and Pattern Recognition, CVPR 2019, Long Beach, CA, USA, June 16-20, 2019*, pages 2700–2709. Computer Vision Foundation / IEEE, 2019. doi: 10.1109/CVPR.2019.00281. URL http://openaccess.thecvf.com/content_CVPR_2019/html/Tang_DeFusionNET_Defocus_Blur_Detection_via_Recurrently_Fusing_and_Refining_Multi-Scale_CVPR_2019_paper.html.
- [65] Chang Tang, Xinzhong Zhu, Xinwang Liu, Lizhe Wang, and Albert Y. Zomaya. Defusionnet: Defocus blur detection via recurrently fusing and refining multi-scale deep features. In *IEEE Conference on Computer Vision and Pattern Recognition, CVPR 2019, Long Beach, CA, USA, June 16-20, 2019*, pages 2700–2709. Computer Vision Foundation / IEEE, 2019. doi: 10.1109/CVPR.2019.00281. URL http://openaccess.thecvf.com/content_CVPR_2019/html/Tang_DeFusionNET_Defocus_Blur_Detection_via_Recurrently_Fusing_and_Refining_Multi-Scale_CVPR_2019_paper.html.
- [66] Chiheb Trabelsi, Olexa Bilaniuk, Ying Zhang, Dmitriy Serdyuk, Sandeep Subramanian, João Felipe Santos, Soroush Mehri, Negar Rostamzadeh, Yoshua Bengio, and Christopher J. Pal. Deep complex networks. In *6th International Conference on Learning Representations, ICLR 2018, Vancouver, BC, Canada, April 30 - May 3, 2018, Conference Track Proceedings*. OpenReview.net, 2018. URL <https://openreview.net/forum?id=H1T2hmZAb>.
- [67] Quoc-Huy Trinh, Nhat-Tan Bui, Trong-Hieu Nguyen Mau, Minh-Van Nguyen, Hai-Minh Phan, Minh-Triet Tran, and Hai-Dang Nguyen. M2unet: Metaformer multi-scale upsampling network for polyp segmentation. In *31st European Signal Processing Conference, EUSIPCO 2023, Helsinki, Finland, September 4-8, 2023*, pages 1115–1119. IEEE, 2023. doi: 10.23919/EUSIPCO58844.2023.10290110. URL <https://doi.org/10.23919/EUSIPCO58844.2023.10290110>.
- [68] Quoc-Huy Trinh, Hai-Dang Nguyen, Nguyen Ngoc Bao Tram, Debesh Jha, Ulas Bagci, and Minh-Triet Tran. Sam-eg: Segment anything model with egde guidance framework for efficient polyp segmentation. In *35th British Machine Vision Conference 2024, BMVC 2024, Glasgow, UK, November 25-28, 2024*. BMVA, 2024. URL <https://papers.bmvc2024.org/0472.pdf>.
- [69] Simon Vandenhende, Stamatios Georgoulis, Wouter Van Gansbeke, Marc Proesmans, Dengxin Dai, and Luc Van Gool. Multi-task learning for dense prediction tasks: A survey. *IEEE Trans. Pattern Anal. Mach. Intell.*, 44(7):3614–3633, 2022. doi: 10.1109/TPAMI.2021.3054719. URL <https://doi.org/10.1109/TPAMI.2021.3054719>.
- [70] T. F. Y. Vicente, Le Hou, Chen-Ping Yu, Minh Hoai, and Dimitris Samaras. Large-scale training of shadow detectors with noisily-annotated shadow examples. In *European Conference on Computer Vision*, 2016. URL <https://api.semanticscholar.org/CorpusID:17623309>.

- [71] Jifeng Wang, Xiang Li, and Jian Yang. Stacked conditional generative adversarial networks for jointly learning shadow detection and shadow removal. In *Proceedings of the IEEE Conference on Computer Vision and Pattern Recognition (CVPR)*, June 2018.
- [72] Junke Wang, Zuxuan Wu, Jingjing Chen, Xintong Han, Abhinav Shrivastava, Ser-Nam Lim, and Yu-Gang Jiang. Objectformer for image manipulation detection and localization. In *IEEE/CVF Conference on Computer Vision and Pattern Recognition, CVPR 2022, New Orleans, LA, USA, June 18-24, 2022*, pages 2354–2363. IEEE, 2022. doi: 10.1109/CVPR52688.2022.00240. URL <https://doi.org/10.1109/CVPR52688.2022.00240>.
- [73] Yue Wu, Wael AbdAlmageed, and Premkumar Natarajan. Mantra-net: Manipulation tracing network for detection and localization of image forgeries with anomalous features. In *IEEE Conference on Computer Vision and Pattern Recognition, CVPR 2019, Long Beach, CA, USA, June 16-20, 2019*, pages 9543–9552. Computer Vision Foundation / IEEE, 2019. doi: 10.1109/CVPR.2019.00977. URL http://openaccess.thecvf.com/content_CVPR_2019/html/Wu_ManTra-Net_Manipulation_Tracing_Network_for_Detection_and_Localization_of_Image_CVPR_2019_paper.html.
- [74] Saurabh Yadav and Koteswar Rao Jerripothula. Fccns: Fully complex-valued convolutional networks using complex-valued color model and loss function. In *IEEE/CVF International Conference on Computer Vision, ICCV 2023, Paris, France, October 1-6, 2023*, pages 10655–10664. IEEE, 2023. doi: 10.1109/ICCV51070.2023.00981. URL <https://doi.org/10.1109/ICCV51070.2023.00981>.
- [75] Saurabh Yadav, Avi Gupta, and Koteswar Rao Jerripothula. SAMwave: wavelet-driven feature enrichment for effective adaptation of segment anything model. In *36th British Machine Vision Conference, BMVC 2025, Sheffield, UK, November 24-27, 2025*. BMVA Press, 2025.
- [76] Bowen Yin, Xuying Zhang, Qibin Hou, Bo-Yuan Sun, Deng-Ping Fan, and Luc Van Gool. Camoformer: Masked separable attention for camouflaged object detection. *arXiv preprint arXiv:2212.06570*, 2022.
- [77] Wenda Zhao, Fan Zhao, Dong Wang, and Huchuan Lu. Defocus blur detection via multi-stream bottom-top-bottom fully convolutional network. In *2018 IEEE Conference on Computer Vision and Pattern Recognition, CVPR 2018, Salt Lake City, UT, USA, June 18-22, 2018*, pages 3080–3088. Computer Vision Foundation / IEEE Computer Society, 2018. doi: 10.1109/CVPR.2018.00325. URL http://openaccess.thecvf.com/content_cvpr_2018/html/Zhao_Defocus_Blur_Detection_CVPR_2018_paper.html.
- [78] Wenda Zhao, Bowen Zheng, Qiuhua Lin, and Huchuan Lu. Enhancing diversity of defocus blur detectors via cross-ensemble network. In *IEEE Conference on Computer Vision and Pattern Recognition, CVPR 2019, Long Beach, CA, USA, June 16-20, 2019*, pages 8905–8913. Computer Vision Foundation / IEEE, 2019. doi: 10.1109/CVPR.2019.00911. URL http://openaccess.thecvf.com/content_CVPR_2019/html/Zhao_Enhancing_Diversity_of_Defocus_Blur_Detectors_via_Cross-Ensemble_Network_CVPR_2019_paper.html.

- [79] Wenda Zhao, Xueqing Hou, You He, and Huchuan Lu. Defocus blur detection via boosting diversity of deep ensemble networks. *IEEE Trans. Image Process.*, 30: 5426–5438, 2021. doi: 10.1109/TIP.2021.3084101. URL <https://doi.org/10.1109/TIP.2021.3084101>.
- [80] Wenda Zhao, Cai Shang, and Huchuan Lu. Self-generated defocus blur detection via dual adversarial discriminators. In *IEEE Conference on Computer Vision and Pattern Recognition, CVPR 2021, virtual, June 19-25, 2021*, pages 6933–6942. Computer Vision Foundation / IEEE, 2021. doi: 10.1109/CVPR46437.2021.00686. URL https://openaccess.thecvf.com/content/CVPR2021/html/Zhao_Self-Generated_Defocus_Blur_Detection_via_Dual_Adversarial_Discriminators_CVPR_2021_paper.html.
- [81] Quanlong Zheng, Xiaotian Qiao, Ying Cao, and Rynson W. H. Lau. Distraction-aware shadow detection. In *IEEE Conference on Computer Vision and Pattern Recognition, CVPR 2019, Long Beach, CA, USA, June 16-20, 2019*, pages 5167–5176. Computer Vision Foundation / IEEE, 2019. doi: 10.1109/CVPR.2019.00531. URL http://openaccess.thecvf.com/content_CVPR_2019/html/Zheng_Distraction-Aware_Shadow_Detection_CVPR_2019_paper.html.
- [82] Lei Zhu, Ke Xu, Zhanghan Ke, and Rynson W. H. Lau. Mitigating intensity bias in shadow detection via feature decomposition and reweighting. In *2021 IEEE/CVF International Conference on Computer Vision, ICCV 2021, Montreal, QC, Canada, October 10-17, 2021*, pages 4682–4691. IEEE, 2021. doi: 10.1109/ICCV48922.2021.00466. URL <https://doi.org/10.1109/ICCV48922.2021.00466>.
- [83] Lei Zhu, Ke Xu, Zhanghan Ke, and Rynson W. H. Lau. Mitigating intensity bias in shadow detection via feature decomposition and reweighting. In *2021 IEEE/CVF International Conference on Computer Vision, ICCV 2021, Montreal, QC, Canada, October 10-17, 2021*, pages 4682–4691. IEEE, 2021. doi: 10.1109/ICCV48922.2021.00466. URL <https://doi.org/10.1109/ICCV48922.2021.00466>.

A Preliminaries

A.1 Wavelet Transform

Wavelet Transform is a classical image processing technique widely used in image compression to separate the low-frequency approximation and the high-frequency details from the original image. Although the original idea of wavelets was proposed for continuous signals, discrete signals like images can also be transformed using discrete wavelet transform (DWT) and inverse wavelet transform (IWT) to regain the original discrete image. To understand DWT, let us start with an input image $I \in \mathbb{R}^{H \times W \times 3}$, a low pass filter L , and a high pass filter H , where:

$$L = \frac{1}{\sqrt{2}} \begin{bmatrix} 1 & 1 \end{bmatrix} \text{ \& } H = \frac{1}{\sqrt{2}} \begin{bmatrix} 1 & -1 \end{bmatrix}$$

Now, using these two filters, a 2D kernel can be constructed by applying each one row-wise and column-wise. It will result in four kernels of stride 2: LL^T, LH^T, HL^T, HH^T . Using the kernels, we decompose the input I into four subbands of size $H/2 \times W/2$, i.e., $I_{ll}, I_{lh}, I_{hl}, I_{hh}$. Note that the kernels are pairwise orthogonal; a 4×4 invertible matrix can be formed to reconstruct the original image accurately from its low-resolution frequency subbands by IWT.

For complex wavelet transform, we replace real-valued wavelets with complex-valued wavelets. Generally, it is also implemented using a dual-tree form focusing on the real and imaginary components of the complex-valued output.

B Additional Method details

B.1 Training Objectives

Following [0, 7], we optimize the tasks in SAMWave by minimizing the loss between the predicted binary mask (\hat{m}) and ground truth (m). Specifically, we use binary cross-entropy loss (L_{bce}) [8] for defocus blur detection and forgery detection, balanced binary cross-entropy loss (L_{bbce}) for shadow detection and summation of binary cross-entropy and intersection-over-union loss ($L_{bbce} + L_{iou}$) for camouflaged object detection. The loss functions are formulated below as follows:

$$\mathcal{L}_{bce}(\hat{m}, m) = -(m * \log(\hat{m}) + (1 - m) * \log(1 - \hat{m})) \quad (1)$$

$$\begin{aligned} \mathcal{L}_{bbce}(\hat{m}, m) = & -\zeta * (m * \log(\hat{m}) \\ & + (1 - m) * \log(1 - \hat{m})) \end{aligned} \quad (2)$$

$$\zeta = \frac{\sum m + \varepsilon}{\sum m + \sum (1 - m) + \varepsilon} \quad (3)$$

$$\mathcal{L}_{iou}(\hat{m}, m) = 1 - \frac{\sum(\hat{m} * m)}{\sum(\hat{m} + m) - \sum(\hat{m} * m)} \quad (4)$$

C Additional Experimental Results

C.1 Datasets

The train and test split for all tasks are shown in Tab. 7.

Table 7: Overview of the datasets used for training and evaluation of our proposed method. In the following table if the training images are “-”, then the dataset is only used for testing.

Tasks	Datasets	Training Images	Testing Images
Forgery Detection	CASIA [14]	5213	921
	IMD20 [46]	-	2010
Shadow Detection	ISTD [41]	1330	540
	SBU [41]	4089	638
Defocus Blur Detection	CUHK[56]	604	100
	DUT[47]	-	500
Camouflaged Object Detection	COD10K [47]	3040	2026
	CAMO [50]	1000	250
	CHAMELEON[50]	-	76
PolyP Detection	CVC-ClinicDB [0]	550	62
	ColonDB [53]	-	380
	Kvasir-SEG [26]	900	100
	ETIS[59]	-	196

C.2 Forgery Detection

Following [0, 57], we evaluate on CASIA [14] and IMD20 [46]. Metrics: pixel-level AUC and \mathcal{F}_1 score. We compare our approach with existing task-specific methods [40, 42, 58, 72, 73] and efficient tuning methods [57]. As shown in Tab. 8, our adaptive approach significantly outperforms prior approaches across the board. Notably, using the SAM backbone in conjunction with *Coiflet* and *Haar* wavelets, our adaptive framework achieves particularly strong performance, demonstrating its effectiveness in high-frequency, detail-sensitive tasks such as image forgery detection.

Table 8: Comparison of state-of-the-art approaches on forgery detection. (■: best, ■: second best)

Method	IMD20	
	$\mathcal{F}1 \uparrow$	AUC \uparrow
ManTra ⁽²⁰¹⁹⁾ [13]	-	0.748
SPAN ⁽²⁰²⁰⁾ [22]	-	0.750
PSCCNet ⁽²⁰²²⁾ [33]	-	0.806
TransForensics ⁽²⁰²¹⁾ [20]	-	0.848
ObjectFormer ⁽²⁰²²⁾ [27]	-	0.821
EVP ⁽²⁰²³⁾ [37]	0.443	0.807
Real-valued Adapters		
SAM as backbone		
Ours (daubechies)	0.539	0.874
Ours (coiflet)	0.626	0.902
Ours (haar)	0.614	0.903
Ours (symlet)	0.607	0.900
SAM2 as backbone		
Ours (daubechies)	0.132	0.500
Ours (coiflet)	0.416	0.658
Ours (haar)	0.131	0.903
Ours (symlet)	0.607	0.900